IEEE Access
Multidisciplinary | Rapid Review | Open Access Journal

Received 17 June 2022, accepted 28 June 2022, date of publication 4 July 2022, date of current version 11 July 2022.

Digital Object Identifier 10.1109/ACCESS.2022.3187985

RESEARCH ARTICLE

Device-Free Indoor Localization of CSI Based on Limited Penetrable Horizontal Visibility Graph

YING LIU AND GUOQING LI
School of Electronic and Information Engineering, Liaoning Technical University, Huludao 125105, China
Corresponding author: Guoqing Li (lgqcommunication@126.com)

This work was supported in part by the National Key Research and Development Program of China under Grant 2018YFB1403303, and in part by the Natural Science Foundation of Liaoning Province under Grant 2019-ZD-0038.

ABSTRACT Most of the current indoor localization methods based on channel state information (CSI) utilize the amplitude and phase of each subcarrier individually as location fingerprints, but the correlation between adjacent subcarriers also contains essential location information. Therefore, this paper proposes a device-free indoor localization method based on CSI and limited penetrable horizontal visibility graph (LPHVG), which does not require the subject to carry a device and can be implemented with only a single access point (AP). Firstly, we model the frequency correlation between subcarriers by LPHVG algorithm and construct a CSI-based complex network. Secondly, the topology of the complex network is utilized to analyze the relationship between CSI adjacent subcarriers and extract network features, which are combined with statistical features as fingerprint information to characterize different locations. Finally, the method is combined with support vector regression (SVR) to realize indoor localization in different environments. The experimental results show that the proposed method can significantly improve the localization accuracy, and has an excellent performance in different indoor scenarios.

INDEX TERMS Device-free localization, channel state information, limited penetrable horizontal visibility graph, support vector regression.

I. INTRODUCTION

With the popularity of mobile technology and wireless devices, location-based services are increasingly relevant to people's daily lives, such as security enforcement, intelligent healthcare, vehicle parking management, and museum visitor guides. Although Global Position System (GPS) has excellent localization and tracking in outdoor environments [1], it often performs less well when applied to indoor localization. Therefore, indoor localization techniques have been studied by a wide range of people [2]–[5]. Many indoor localization methods require the tracked object to carry a specific mobile device [6], while the tracked object cannot bring any device in many cases. Therefore, designing efficient and feasible device-free localization methods is a current challenge.

The associate editor coordinating the review of this manuscript and approving it for publication was Rui Wang.

Most previous device-free localization technologies are based on Bluetooth [7], radio frequency identification [8], ultra-wideband [9], and geomagnetic [10], but the complex equipment limit the usage of these technologies. With the widespread deployment of Wi-Fi networks, Wi-Fi-based localization technology has attracted increasing attention in recent years. The method of comparing pre-constructed radio maps to determine a person's location by changing channel characteristics of Wi-Fi signals is known as the fingerprint method. Since Wi-Fi Received Signal Strength (RSS) is easily accessible, conventional indoor localization systems [11]–[14] utilize RSS as fingerprint information. For example, the Radar system [13] is the pioneer of the RSS-based fingerprint localization system, which utilizes a deterministic approach for location estimation. The Horus system [14] utilizes a probabilistic approach for location estimation based on RSS, which has some improvement over Radar in terms of localization accuracy. However, the presence of effects such as indoor multipath propagation and

shadow fading leads to high volatility of RSS as a simple superposition of multipath components, which cannot meet the requirements of high accuracy localization. With the innovation of technical means, we can obtain CSI signals from more advanced Wi-Fi network interface cards, such as the Inter Wi-Fi Link 5300 network card [15], by modifying the device drivers. Unlike RSS from the media access control (MAC) layer, channel state information (CSI) is based on orthogonal frequency division multiplexing (OFDM) from the physical layer. The fine-grained characteristics can more accurately depict changes in channel states, which makes it highly attractive for realizing high-precision indoor localization technology. Therefore, this paper takes CSI fingerprint as the research subject.

However, most existing methods utilize only the amplitude and phase of each CSI subcarriers alone to construct fingerprint information, ignoring the essential location information contained in the correlation of adjacent subcarriers. Therefore, this paper utilizes the limited penetrable horizontal visibility graph (LPHVG) algorithm [16] to model the correlation between subcarriers and analyze the characteristics between adjacent subcarriers using the topology of complex networks. The central idea is to convert LPHVG time series into CSI frequency-domain series, construct a complex network with subcarriers as network nodes and geometric visual visibility as edges, extract corresponding network features and combine statistical characteristics as fingerprint information on this basis, and finally realize indoor localization based on support vector regression (SVR). By combining the intra-subcarrier statistical features and inter-subcarrier network features, the connection between CSI subcarriers is revealed, the correlation between fingerprint features and location information is enhanced, and the localization performance of the algorithm is improved.

The contributions made in this paper are as follows:

1) We propose a LPHVG-based method for device-free indoor localization of CSI. The method solves the problem of poor localization performance due to using only a single subcarrier by exploring the correlation between adjacent subcarriers.

2) A fingerprint pattern combining network features and statistical features, containing both intra- and inter-subcarrier location information and can effectively improve the localization accuracy.

3) Implementing localization in three indoor environments with device-free and single AP. The results show that the method outperforms existing indoor localization methods and has good anti-noise performance for complex environments.

The rest of this paper is organized as follows. In Section II, we provide an overview of the work related to CSI indoor localization and visibility graph technologies. In Section III, we present the basic theory about CSI and LPHVG. In Section IV, we elaborate the methodology proposed in this paper. In Section V, we describe the experimental environment and make a performance analysis. In Section VI, we summarize the paper.

II. RELATED WORD

This section presents the work related to CSI-based fingerprint localization and visibility graph techniques, respectively.

A. CSI-BASED FINGERPRINT LOCALIZATION

FIFS [17] processed CSI amplitude by frequency diversity and spatial diversity, and mapped the amplitude into fingerprints using a probabilistic model to construct a fingerprint database, which has an average error of about 1 m. DeepFi [18] utilized deep learning for training 90 subcarriers of three antennas through a deep network to obtain fingerprints with the best weights. FapFi [19] filtered the amplitude and phase information, and realizes the passive indoor positioning based on Bayesian classification. BiLoc [20] proposed to develop bimodal CSI using a bimodal deep autoencoder network, including the average CSI amplitude and phase difference. To address the correlation between features, [21] modeled the fingerprint information at each location as normal distribution and combined it with a weighted plain Bayesian classifier for localization. Reference [22] implemented random forest (RF)-based indoor localization using a random forest model trained in the offline phase as a fingerprint to combat multipath effects. Reference [23] proposed an improved Bayesian localization method, which calculated the mean and standard deviation of different subcarriers to generate a fingerprint database. Reference [24] proposed a time-reversal indoor localization system (TRIPS) that creates a database by mapping physical geographic locations in channel impulse response (CIR) space to logical locations, and then uses fingerprints from unknown locations and fingerprints in the database to evaluate the time-reversal resonating strength (TRRs) and determine the true physical location. The system can achieve 10 cm localization accuracy and zero error rate in a 0.9 m $\times$ 1 m region of interest. Reference [25] made full use of spatial diversity in multiple-input multiple-output (MIMO) Wi-Fi systems to obtain a larger effective bandwidth. During the localization phase, the collected instantaneous CFR is compared with the fingerprint library via TRRs with compensation for residual synchronization errors. Experimental results show that localization accuracy of 1$\sim$2 cm can be achieved at a measurement resolution of 0.5 cm and that the system is robust to environmental dynamics caused by human activity and object motion. This centimeter-level positioning systems have a very small positioning area and a very high resolution. Most of the above works consider only a single subcarrier and ignore the location information between adjacent subcarriers. Indeed, it has been shown in the [26] that the adjacent subcarriers are strongly correlated with each other. Therefore, the study of frequency correlation between subcarriers is helpful to improve positioning performance.

TABLE 1. Comparison of the related works.

	System/Work	Fingerprint/Application	Method
CSI-based	FIFS [17]	Amplitude, Phase	Bayes
	DeepFi [18]	Amplitude	Deep Network
	FapFi [19]	Amplitude, Phase	Bayes
	BiLoc [20]	Amplitude, Phase	Bi-modal deep learning
	D. Man et al. [21]	Amplitude	Weighted Naive Bayes
	Y. Wang et al. [22]	Amplitude	RF
	Z. Wu et al. [23]	Amplitude	Improved Bayes
	Z. Wu et al. [24]	Amplitude, Phase	Time-Reversal (TR)
	C. Chen et al. [25]	Amplitude, Phase	Time-Reversal (TR)
VG-based	L. Lacasa et al. [27]	Put forward the VG	VG
	J. Iacovacci et al. [28]	Picture processing	VG
	Z. Wu et al. [29]	Human body orientation detection	VG
	Z. Wu et al. [30]	Indoor localization	VG
	L. Lacasa et al. [31]	Put forward the HVG	HVG
	S.S. Roy et al. [32]	Discharge detection	HVG
	Y. Luo et al. [33]	Network traffic feature extraction	LPVG
	Y. Lv et al. [16]	Muscle synergy	MLPHVG

B. VISIBILITY GRAPH TECHNIQUES

Complex networks have wide applications in many complex systems analyses, such as aviation networks, social networks, and transportation networks. Also, visibility graph (VG) is an effective method to convert time series data into complex networks. Reference [27] proposed to build VG models of complex networks from time series. Reference [28] utilized VG algorithm for image processing. Reference [29] proposed to utilize VG to model the correlation between CSI subcarriers to achieve the detection of human orientation. Later, VG was suggested to be applied to indoor localization [30]. Reference [31] simplified VG and proposed a horizontal visibility graph (HVG) construction method. Reference [32] combines HVG algorithm with spectral analysis for partial discharge detection. To improve the outlier detection rate of network traffic, Reference [33] proposed the utilization of limited penetrable visibility graph (LPVG) for accurate extraction of network traffic features. Reference [16] further proposed the method of multiscale limited penetrable horizontal visibility graph (MLPHVG) to improve classification accuracy. The above work shows that converting time series data into complex networks using visibility graph-based techniques can reveal intrinsic connections between the data. Table 1 shows the comparison of the related works.

III. PRELIMINARY

A. CHANNEL STATE INFORMATION

The CSI can be acquired through an Intel 5300 NIC. The collected raw CSI belongs to frequency domain data, which reflects the fading state of the signal during the propagation between the transmitter and the receiver. The channel model can be described as:

$$Y = HX + N \tag{1}$$

where X is the transmit signal, Y is the received signal, $H$is the channel matrix, and N is the Gaussian white noise. Therefore, the CSI estimates of all subcarriers can be expressed as:

$$H = \frac{Y}{X} \tag{2}$$

Wireless channels are generally described by the channel impulse response (CIR) to the multipath effect of the channel. Under the assumption of linear time invariance, CIR is expressed as the following (3):

$$h(\tau) = \sum_{i=1}^{l-1} a_i e^{-j\theta_i} \delta(\tau - \tau_i) \tag{3}$$

where a_i, θ_i, and τ_i are the amplitude, phase, and time delay of the i^{th} path, respectively, l is the total number of multipath, and $\delta(\tau)$ is the Dirac function.

The multipath propagation of the signal is manifested in the time domain as time delay expansion, while in the frequency domain, it causes selective fading of the signal. The channel frequency response (CFR) of the wireless channel can be obtained from the CIR by Fourier transform. The CFR can be expressed as:

$$H_i = |H_i| \, e^{\mathrm{j}\sin(\angle H_i)} \tag{4}$$

where $|H_i|$ and $\angle H_i$, denote the amplitude and phase of the i^{th} subcarrier, respectively. The number of subcarriers used is 30.

Due to indoor environmental variations and multipath effects, the attenuation of the signal varies from path to path,

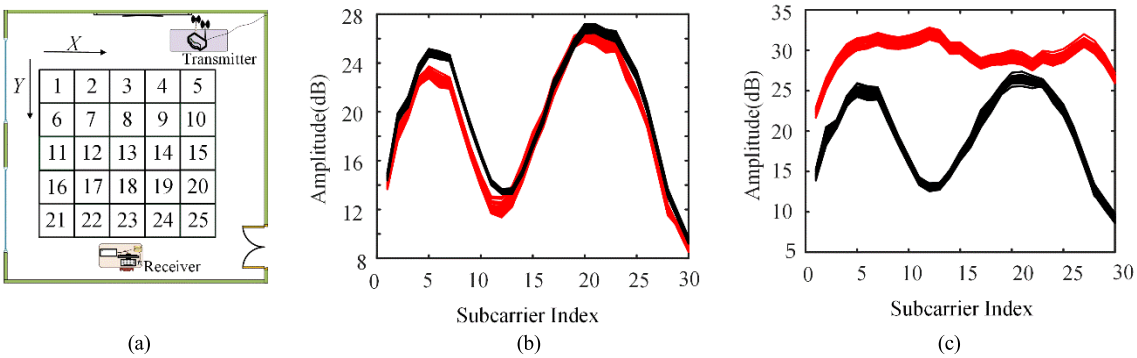

(a) (b) (c)

FIGURE 1. The CSI amplitude comparison. (a) Scene plan. (b) CSI amplitude in the same location. (c) CSI amplitude in different location.

resulting in a distribution structure with corresponding characteristics of the subcarriers. Fig. 1 represents the processed amplitudes in the same and different positions, respectively, when people are present. Fig. 1(a) shows the layout of the indoor environment, Fig. 1(b) shows the amplitude obtained twice when the person is at position 6, and Fig. 1(c) shows the amplitude obtained when the person is at position 6 and position 20 respectively (black represents position 6 and red represents position 20). We can see that the CSI amplitude satisfies the characteristics of being stable at the same location and easily distinguishable at different locations. Therefore, it is feasible to utilize CSI amplitude as a feature of fingerprint localization, which can reflect the change of the location of the target to be measured in the area of interest.

Combining amplitude and phase provides a more comprehensive characterization of fingerprint information and improves localization accuracy compare to use only amplitude or phase. However, the phase information is shifted due to carrier frequency offset (CFO) and sampling frequency offset (SFO), and the received raw phase information is cluttered. Therefore, this paper corrects the phase, and the correction process is described in Section IV-A.

B. LPHVG INTRODUCTION

In the LPHVG model, each time point in the discrete-time series is defined as a network node. The concatenation between corresponding values satisfying the visibility criterion is defined as the network concatenation edge. Define L_p as the limited penetrable visibility distance and T_f as the truncation number, the visibility criterion of LPHVG is that if any two nodes$(t_a, y_a)$and(t_b, y_b)in the time series are separated by$S$nodes and are visible to each other, then there existT_f $\left(0 \leq T_f \leq L_p\right)$observations$(t_i, y_i)$between these two nodes, satisfying:

$$y_i > y_a \text{ or } y_i > y_b, \quad \forall t_i \in (t_a, t_b) \tag{5}$$

The remaining $S - T_f$ points $\left(t_j, y_j\right)$ satisfy:

$$y_j < \min\left(y_a, y_b\right), \quad \forall t_j \in (t_a, t_b) \tag{6}$$

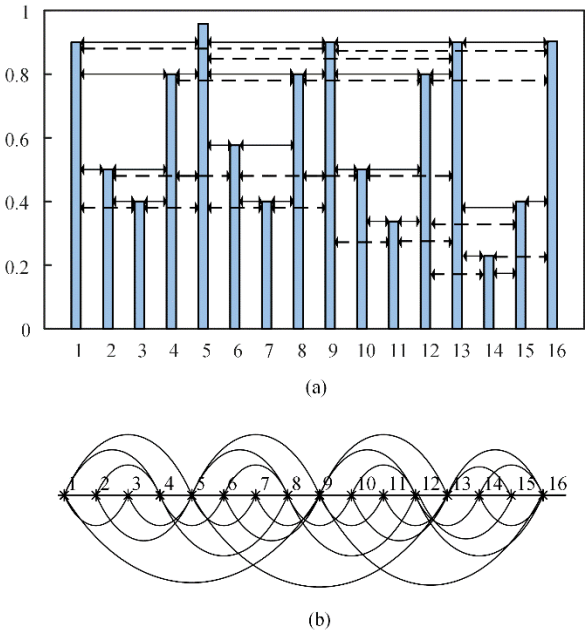

FIGURE 2. Example of LPHVG analysis when $L_p = 1$. (a) Time series data. (b) Constructed LPHVG network.

Fig. 2 shows the network construction method of the LPHVG algorithm when $L_p = 1$. In Fig. 2(a), X-axis is the time series, Y-axis is the corresponding value, and Fig. 2(b) is the complex network constructed according to the visual criteria. The 16 points in Fig. 2(b) correspond to the 16 network nodes in Fig. 2(a), and the lines between the points in Fig. 2(b) correspond to the network edges between the 16 values in Fig. 2(a). We first construct the network connected edges between the network nodes in Fig. 2(a) by the visibility criterion, and then obtain the complex network in Fig. 2(b) by corresponding the network nodes and the network connected edges one by one.

Compared with the LPVG, the LPHVG reduces the complexity of network construction while preserving the inheritance of network characteristics due to the simplified visibility criterion. It also has tighter network indirection

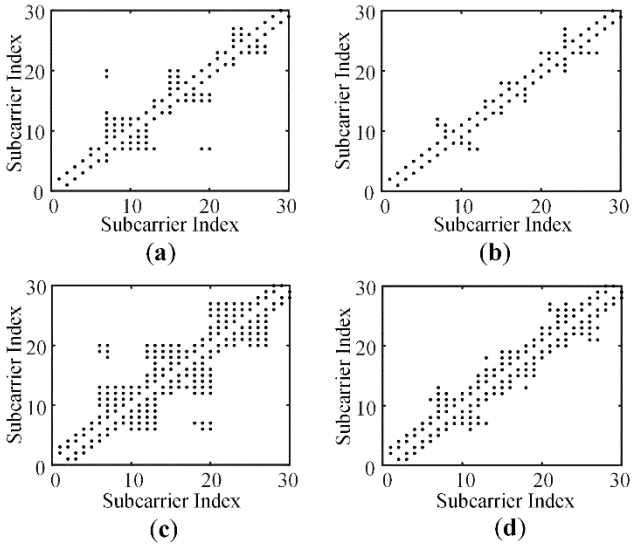

FIGURE 3. Adjacency matrix comparison of four visibility graph methods. (a) Adjacency matrix of VG. (b) Adjacency matrix of HVG. (c) Adjacency matrix of LPVG. (d) Adjacency matrix of LPHVG.

and broader visibility than VG and HVG. Usually, a more significant average degree value of a network node represents tighter network connectivity, which proves that the algorithm can inherit the characteristics between the original frequency sequences well. This paper analyzes the network degree distribution of VG, HVG, LPVG and LPHVG models by adjacency matrix. Fig. 3(a)-(d) respectively represents the adjacency matrices of VG, HVG, LPVG, and LPHVG. The horizontal and vertical coordinates indicate the subcarrier indexes. We can see that the node average degree value of the LPVG-based CSI complex network is greater than that of VG, HVG, and LPHVG, implying that it outperforms other algorithms in terms of network connectivity. However, the high complication of the LPVG visibility criterion also adds to the algorithm complexity. We note that the LPHVG algorithm is higher than the VG and HVG algorithms in terms of frequency feature inheritance and significantly reduces the complexity of network construction compared to LPVG due to its visibility criterion judgment. Therefore, considering the network performance and algorithm complexity, we choose the LPHVG algorithm to construct CSI complex networks and explore the frequency correlation among subcarriers.

IV. SYSTEM MODEL

To more accurately represent the mapping relationship between location and fingerprint, a complex network of CSI based on LPHVG is constructed in this paper. The precise location of indoor people is achieved by analyzing the relationship between adjacent subcarriers of CSI and extracting relevant features. Fig. 4 shows the architecture of the proposed scheme. Firstly, we collect data at different positions in the positioning area, and perform phase correction and filtering on the original CSI. Then the statistical features are extracted from the pre-processed CSI, while a complex

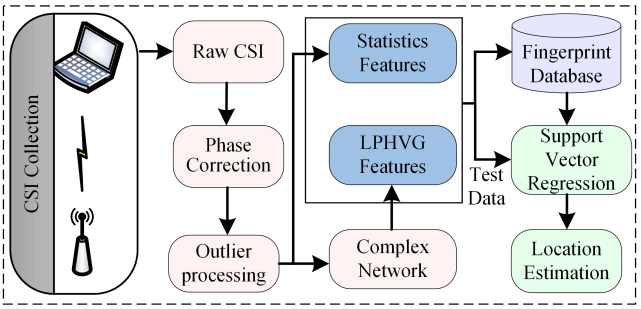

FIGURE 4. System Architecture.

network based on LPHVG is constructed and network features are extracted. The obtained feature values are divided into training data and test data according to the scale. The fingerprint library is constructed for the training data. Finally, the location localization in different experimental environments is implemented based on the SVR method.

A. DATA PREPROCESSING

Due to the complexity of the indoor environment, experimental equipment is susceptible to the influence of temperature and humidity of the surrounding environment, so the raw CSI cannot be utilized for localization. Therefore, this paper preprocesses the raw data.

1) PHASE CORRECTION

This paper utilizes the linear fitting method to correct the phase [34], and the measured phase extracted to the i^{th} subcarrier is expressed as $\angle\tilde{\phi}_i$, which can be expressed by (7) as:

$$\angle\tilde{\phi}_i = \angle\phi_i + 2\pi\frac{m_i}{k}\Delta t + \beta + Z \tag{7}$$

where $\angle\phi_i$ is the actual phase, k is the Fourier transform length, m_i denotes the carrier number of the i^{th} subcarrier, $i = 1, 2, \ldots, 30$, Δt means the time delay caused by the SFO, β expresses the phase shift caused by the CFO, and Z denotes noise phase.

Since $2\pi\frac{m_i}{k}\Delta t + \beta$ is a linear function on m_i, (7) can be written as:

$$\angle\tilde{\phi}_i = \angle\tilde{\phi} - km_i - b \tag{8}$$

where $\angle\tilde{\phi}$ denotes the corrected phase, k denotes the slope, and b denotes the intercept. k and b are marked as:

$$k = \frac{\left|\angle\tilde{\phi}_{30} - \angle\tilde{\phi}_1\right|}{m_{30} - m_1} \tag{9}$$

$$b = \frac{1}{30}\sum_{i=1}^{30}\angle\tilde{\phi}_i \tag{10}$$

With the above correction algorithm, the errors in the original phase due to CFO and SFO are removed, and the phase values are in the range of $[-\pi, \pi]$.

2) OUTLIER PROCESSING

For the outliers present in the original data, this paper utilizes the Hampel filter to reject them, and the principle is as follows:

$$csi_i^n = \begin{cases} mean_i \left| csi_i^n - mean_i \right| > 3std_i \\ csi_i^n \left| csi_i^n - mean_i \right| \leq 3std_i \end{cases} \tag{11}$$

where csi_i^n denotes the CSI of the i^{th} subcarrier of the n^{th} sample, *mean* denotes the mean value, and *std* is the standard deviation.

B. LPHVG-BASED CSI NETWORK CONSTRUCTION

To explore the correlation between subcarriers and mine the location information contained between subcarriers, this paper maps CSI to complex networks from the perspective of frequency sequences, using the LPHVG algorithm as a visual criterion. The specific construction method of CSI complex networks is divided into two steps:

(1) Constructing the node-set: The frequency sequence can be expressed as $\{csi_i\}$, $i \in (1, N)$, N denotes its length, i.e., the number of subcarriers. Define each subcarrier as a network node and construct a CSI network node-set with $N = 30$.

(2) Constructing the connected edge set: Firstly, adjacent subcarriers are connected by horizontal lines. Secondly, if any two non-adjacent subcarriers meet the LPHVG visibility criterion, they are connected by horizontal lines.

The visibility criterion of LPHVG: Define$L_p$as the limited penetrable visibility distance and T_f as the truncation number, if any two nodes $(f_a, csi_a)$and (f_b, csi_b) in the time series are separated by S nodes and are visible to each other, then there exist $T_f \left(0 \leq T_f \leq L_p\right)$ observations (f_i, csi_i) between these two nodes, satisfying:

$$csi_i > csi_a \text{ or } csi_i > csi_b, \quad \forall f_i \in (f_a, f_b) \tag{12}$$

The remaining $S - T_f$ points $\left(f_j, csi_j\right)$, satisfying:

$$csi_i < \min\left(csi_a, csi_b\right), \quad \forall f_j \in (f_a, f_b) \tag{13}$$

where f_i denotes the frequency of the i^{th} subcarrier, and csi_i indicates amplitude or phase.

Fig. 5 shows the complex network of CSI constructed based on the LPHVG algorithm. Where the horizontal coordinates denote the frequency sequence, and the vertical coordinates denote the corresponding amplitude or phase. Specifically, we first treat the 30 subcarriers of CSI as network nodes, i.e., the horizontal coordinates represent the frequency sequence, and the corresponding amplitude or phase of each subcarrier as the corresponding value of the network nodes, i.e., the vertical coordinates represent the amplitude or phase. Then, according to the visibility criterion described in the previous section, the values between two nodes in the coordinate system that satisfy the LPHVG visibility criterion are concatenated, and all network nodes are traversed in this method in turn. Finally, the network nodes in the constructed coordinate system and the connected edges of the network

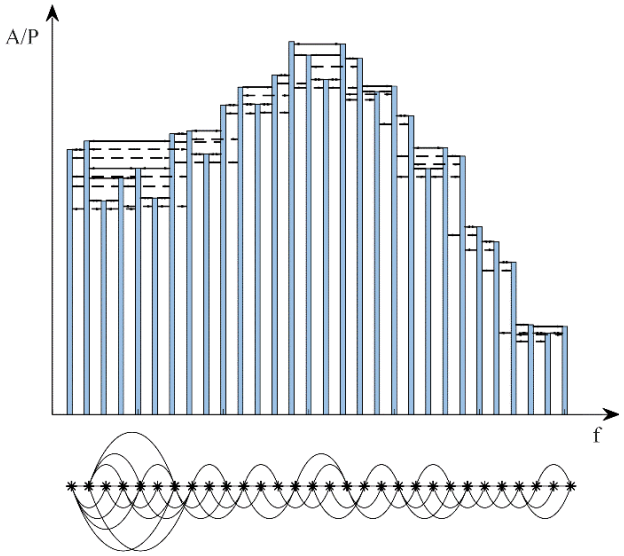

FIGURE 5. CSI network construction of the LPHVG algorithm.

are matched one by one to obtain the final complex network. We build the CSI frequency domain data as a loop-free and directionless complex network by using subcarriers as network nodes and establishing connections between nodes according to the LPHVG visibility criterion. Further, the CSI network is analyzed by existing network analysis techniques, and then the correlation between subcarriers can be fully explored.

C. FINGERPRINT FEATURES

1) NETWORK FEATURE EXTRACTION

In this paper, the features of the pre-processed CSI are extracted from intra-subcarrier and inter-subcarrier, respectively. For the intra-subcarrier features, we utilize the statistical characteristics of each subcarrier, i.e., mean and standard deviation. For the inter-subcarrier features, we characterize the topology of the complex network by the topological parameters of the corresponding matrix. The degree deviation, clustering coefficient entropy, congruence coefficient, and average weight degree [33], [35] are chosen to characterize the network of CSI data, with the following equations:

(1) Degree deviation. The degree D_i of node i is defined as the number of edges connected to the node, which reflects the degree of association of nodes in a complex network, and D_{std} is the standard deviation of the degrees of all nodes in the network, which describes the degree of connection sparsity of the complex network. The degree deviation is calculated by the formula:

$$D_{std} = \left(\frac{\sum_{i=1}^{N} \left(D_i - \overline{D}\right)^2}{N - 1} \right)^{\frac{1}{2}} \tag{14}$$

where $\bar{D} = 1/V \sum D_i$ denotes the average degree and N is the total number of nodes.

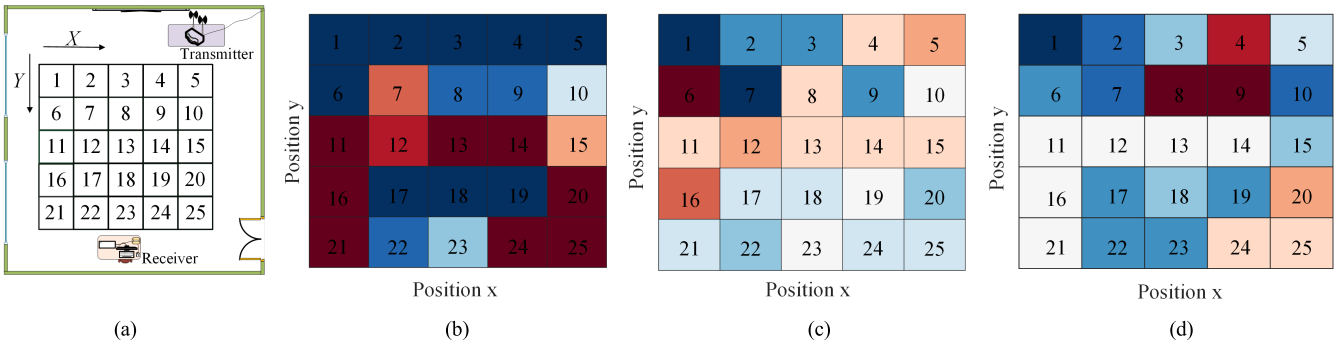

FIGURE 6. Description of characteristic advantages. (a) Scene plan. (b) amplitude. (c) statistical features. (d) network features.

(2) Clustering coefficient entropy. The entropy of clustering coefficients is utilized to describe the clustering characteristics of the network nodes, and its formula is:

$$\begin{cases} C_i = \dfrac{2\xi_i}{D_i\left(D_i-1\right)} \\ P_{C,i} = \dfrac{C_i}{\sum_{i=1}^{N} C_i} \end{cases}$$
$$E_C = -\sum_{i=1}^{N}\left(P_{C,i}\right)\log\left(P_{C,i}\right) \tag{15}$$

where C_i is the clustering coefficient, ξ_i is the total number of edges of all neighboring nodes connected to node i. $P_{C,i}$ is the clustering coefficient probability, E_C is the clustering coefficient entropy, and N is the total number of nodes.

(3) Congruence coefficient. The Pearson correlation coefficient of degree is utilized to describe the degree correlation of the network, i.e., the congruence coefficient R, which is defined as:

$$R = \frac{E^{-1}\sum_i D_{1,i}D_{2,i} - \left[E^{-1}\sum_i \frac{1}{2}\left(D_{1,i}+D_{2,i}\right)\right]^2}{E^{-1}\sum_i\left(D_{1,i}^2+D_{2,i}^2\right) - \left[E^{-1}\sum_i \frac{1}{2}\left(D_{1,i}+D_{2,i}\right)\right]^2} \tag{16}$$

where $D_{1,i}$ and $D_{2,i}$ is the degree of the two nodes connected by edge i and E is the total number of edges.

(4) Average weighted degree. The weighted degree represents the connection density of the complex network, and the larger the mean value proves that the edge connection structure is denser. The average weight degree $\overline{w}$ is extracted by the following equation:

$$\begin{cases} w_{ij} = \arctan\dfrac{csi(f_j) - csi(f_i)}{f_j - f_i} \\ \overline{w} = \dfrac{1}{E}\sum_{i=1}^{E}\sum_{j\in B(i)} w_{ij} \end{cases} \tag{17}$$

where w_{ij} represents the weights of the edges between nodes$i$ and j, f_i is the corresponding subcarrier frequency, csi is the amplitude or phase, $B\,(i)$ is the set sum of all edges connected to the node i, and E is the total number of edges.

Fingerprint database is created by adding category labels and location information to each set of network features and statistical features obtained, and the fingerprint database F is:

$$F = [CSI_{\text{Net}}\ CSI_{\text{Sta}}\ M\ L] \tag{18}$$

where CSI_{Net} denotes the network matrix, CSI_{Sta} denotes the statistical matrix, n is the number of samples, M is the category label corresponding to the fingerprint, and L is the coordinate corresponding to the fingerprint of the form $L_i = (x_i, y_i)$.

2) ADVANTAGES OF SELECTED FEATURES

To verify that the features proposed in this paper can be used as locating fingerprints, an open indoor scene is divided into 25 location cells. Fig. 6(a) is the plan of the scene. The environment is quiet and empty, we only set up the sending and receiving equipment and related personnel, and the size of each location unit is 0.8m×0.8m. Fig. 6(b), Fig. 6(c) and Fig. 6(d) respectively show the thermal diagram in which amplitude, statistical features, and network features are used as fingerprint information in this scene. It can be seen from the figure that when fingerprint positioning is carried out, taking amplitude as fingerprint information will produce serious spatial ambiguity, which will lead to wrong location classification. Both statistical features and network features show the good mapping between different locations and fingerprints, proving that both fingerprint features can be used for positioning. At the same time, the respective positions of the two features and the mapping relationship between the fingerprints are different, indicating that the two features represent the CSI fingerprint from different perspectives and respectively represent different fingerprint information. For example, in Fig. 6(c), position 5 and position 12 are far apart but have similar fingerprint information, while in Fig. 6(d), the fingerprint information of position 5 and position 12 is quite different. It can be seen that the combination of the two features as a fingerprint can more fully characterize the data and further improve the positioning accuracy.

D. SVR FOR LOCALIZATION

The essence of indoor localization based on CSI fingerprints is to establish the mapping relationship from CSI fingerprint information to the physical location. Deep learning is currently widely used in artificial intelligence and other fields, and has shown good learning ability. However, the method usually requires a large amount of training data, high algorithm complexity and long system running time. In this paper, the number of samples to be processed is small, and there is a large similarity between features. SVR [36] is a regression algorithm that can achieve a nonlinear mapping from input to output, and it has strong generalization and fitting ability. Therefore, this paper utilizes SVR to train the model and predict location.

Each training sample corresponds to a physical location, and the SVR projects the input signal space into a high-dimensional feature space by a nonlinear transformation, where the regression function is:

$$f(r) = w^T r + b \tag{19}$$

where w is a vector indicating the direction of the function, b is a constant indicating its location, and r denotes the training data. T denotes transpose. According to the structural risk minimization principle of SVR, each sample is allowed to have an error not exceeding ε. The excess is captured by the relaxation variables ξ_i and ξ_i^*, which are penalized by the regularization constant C chosen a priori. Thus, the regression problem can be solved as follows:

$$\begin{aligned} &\min \ \frac{1}{2}\|w\|^2 + C\sum_{i=1}^{N}(\xi_i + \xi_i^*), \\ &s.t. \ \begin{cases} (w^T r + b) - c_i \le \varepsilon + \xi_i \\ c_i - (w^T r + b) \le \varepsilon + \xi_i^* \\ \xi_i, \xi_i^*, \varepsilon \ge 0 \end{cases} \end{aligned} \tag{20}$$

where c_i denotes the x (or y) coordinate of the i^{th} location. Using the kernel function to solve-(20), the regression function is obtained as follows:

$$f(r) = \sum_{i=1}^{m}(\alpha_i - \hat{\alpha}_i)K(r_i, r) + b \tag{21}$$

where α_i and $\hat{\alpha}_i$ are Lagrangian multipliers and $K(r_i, r)$ is a kernel function.

To obtain an excellent fitting effect, the radial basis function (RBF) is chosen as the kernel function in this paper, which takes the form of (γ is the kernel parameter):

$$K(r_i, r) = \exp(-\gamma \|r_i - r\|^2), \gamma > 0 \tag{22}$$

In the fingerprint localization algorithm in this paper, the location coordinates have two dimensions, so separate training is required for the x and y coordinates. The test data are fed into the trained model to obtain the estimated coordinates of the point to be located.

V. EXPERIMENT VALIDATION

This section describes the implementation and performance evaluation of the proposed method. Firstly, we describe the experimental configuration and the experimental environment. Then the performance is verified and compared with existing methods. Finally, we analyze the effect of the choice of experimental parameters on the localization performance.

A. EXPERIMENTAL SETUP

The equipment utilized is a desktop computer with an Intel 5300 NIC and Ubuntu 12.04 operating system, with the Linux 802.11n CSI Tool installed to obtain CSI. For the transmitter, a router with the model number TP-LINK is utilized. Two transmitting antennas and three receiving antennas can theoretically acquire data from 2∗3 links, but channel links are often unstable in the actual data acquisition process. Therefore, 1∗3 stable links are extracted in this paper, i.e., link pairs 1-1, 1-2, 1-3. In this paper, an empty room, a conference room, and a corridor are selected as different experimental scenarios, and several 0.8m × 0.8m location grids are arranged. As shown in Fig. 7(a)-(c), Environment 1 is quiet and empty, Environment 2 is placed with several sets of equipment and obstacles, and Environment 3 is narrow and slender and a volunteer was scheduled to pass through the corridor at a frequency of once every minute. In this paper, we set the transmission frequency of data packets in the experiment to 100Hz, and each collection lasts 10 seconds. We get 1000 sets of data at each location as the sample set, and divide them into training and test sets in the ratio of 8:2.

B. PERFORMANCE ANALYSIS

1) FINGERPRINT FEATURES

To verify the effect of intra- and inter-subcarrier features on localization accuracy, we plot the confusion matrix obtained for 25 locations in the empty room under different fingerprint representations based on the SVM classification algorithm. Fig. 8(a)-(c) respectively represents the confusion matrix of network features, statistical features, and combined features, where the x-axis represents the predicted location, the y-axis represents the actual location, and the z-axis represents the predicted frequency. We can see that the LPVHG and Statistics methods may have different misclassification results for the same location, i.e., to a certain extent, they have complementary properties. For example, position 5. The utilization of combined fingerprints, on the other hand, significantly reduces the frequency of misclassification, which means that the network features indicating the correlation between subcarriers and the statistical features of individual subcarriers represent different location information, respectively. Therefore, combining the two components can effectively reduce the frequency of false recognition and improve localization performance.

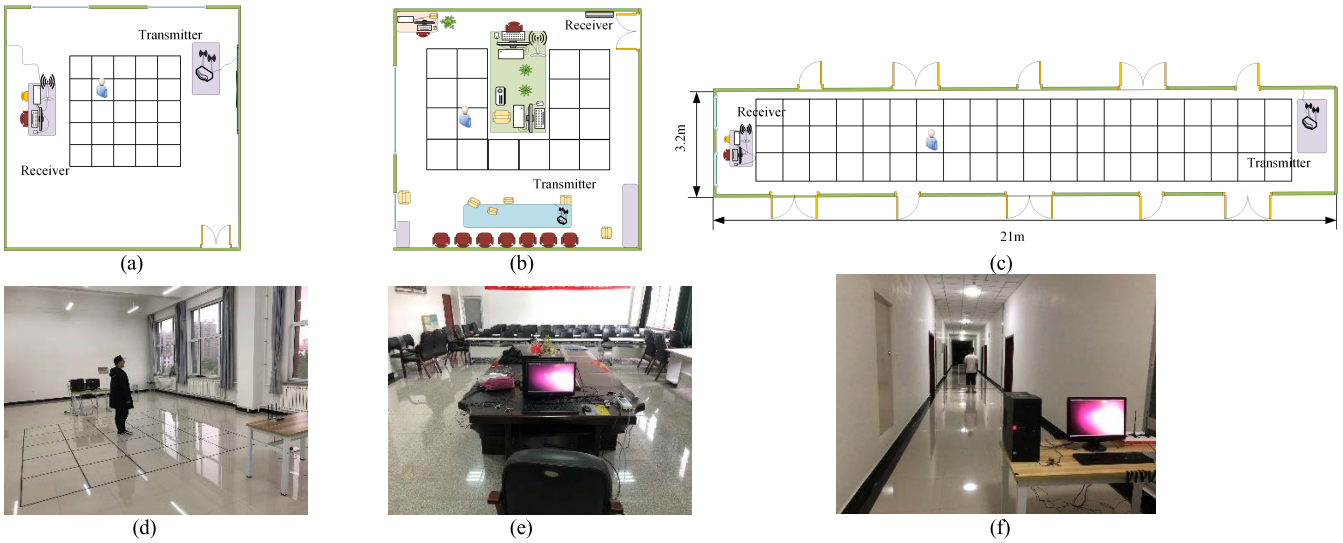

FIGURE 7. Different environments. (a) Plan of empty room. (b) Plan of conference room. (c) Plan of empty corridor. (d) Photograph of empty room. (e) Photograph of conference room. (f) Photograph of corridor.

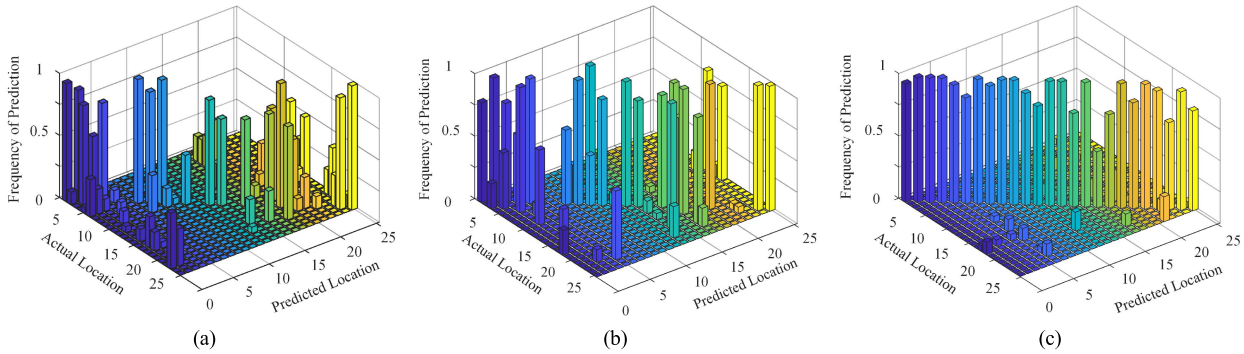

FIGURE 8. The confusion matrix of different fingerprints. (a) Network features. (b) Statistical features. (c) Combined features.

2) COMPARISON OF DIFFERENT FINGERPRINTING METHODS

In this paper, we evaluate the impact of several different fingerprint features on the localization performance as follows:

1. Only-LPHVG method: network features extracted only from the LPHVG algorithm

2. Only-Statistics method: statistical features commonly utilized in existing localization methods, i.e., mean and standard deviation of subcarriers [25]

3. VG and Statistics method: utilizing a combination of VG and statistics as a fingerprint [30]

4. Proposed method: utilizing a combination of LPHVG and Statistics as a fingerprint

We evaluate the performance of different fingerprints in three different environments using the SVR-based localization algorithm. Fig. 9(a)-(c) shows the cumulative distribution function (CDF) of the localization errors obtained for the empty room, the conference room, and the corridor, respectively. From the figure, it can be seen that the error of 80% of the test data of the proposed fingerprint method can be controlled within 0.7m in the empty room, while the positioning accuracy of methods 1, 2 and 3 can be 1.2m, 1m and 0.9m respectively at this percentage; 80% of the test data of the proposed fingerprint method can be controlled within 1m in the conference room, while the positioning accuracy of methods 1, 2 and 3 can be 1.5m, 1.3m and 1.2m respectively at this percentage. The localization accuracy of methods 1, 2, and 3 in this percentage is 1.5m, 1.3m, and 1.2m, respectively; in the corridor, the error of 80% of the test data of the proposed fingerprint method can be controlled within 1.5m, while the localization accuracy of methods 1, 2 and 3 in this percentage is 1.7m, 2m, and 3.1m, respectively. statistics, as shown in Table 2. The results show that the average error and median error of the fingerprint methods proposed in this paper are lower than those of other methods under different experimental environments. We can see that the proposed method outperforms the methods using only-LPHVG and only-Statistics, which indicates that there is indeed important information about the location between

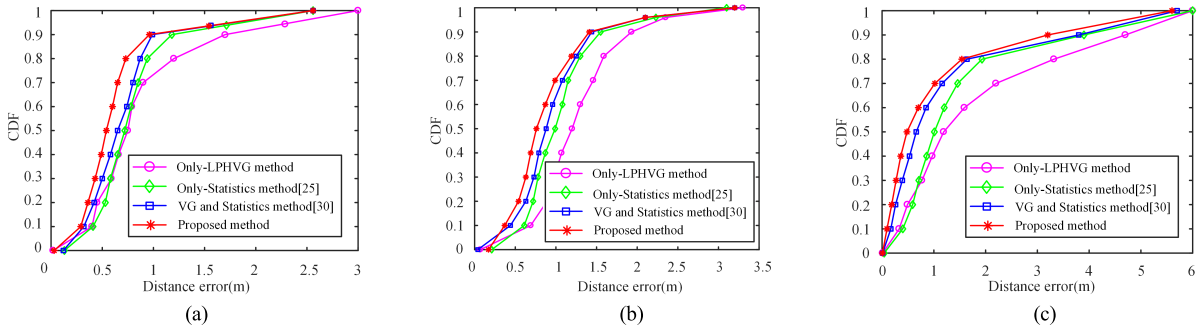

FIGURE 9. CDF of different fingerprint methods in three environments. (a) Empty room. (b) Conference room. (c) Corridor.

TABLE 2. Localization errors of different fingerprinting methods (meters).

	Empty Room		Conference Room		Corridor	
	Mean	**Median**	**Mean**	**Median**	**Mean**	**Median**
Only-LPHVG	0.809	0.728	1.253	1.190	2.042	1.291
Only-Statistical [25]	0.766	0.714	1.049	0.987	1.541	1.098
VG and Statistic [30]	0.710	0.603	0.936	0.875	1.307	0.655
Proposed method	**0.596**	**0.535**	**0.837**	**0.755**	**1.270**	**0.579**

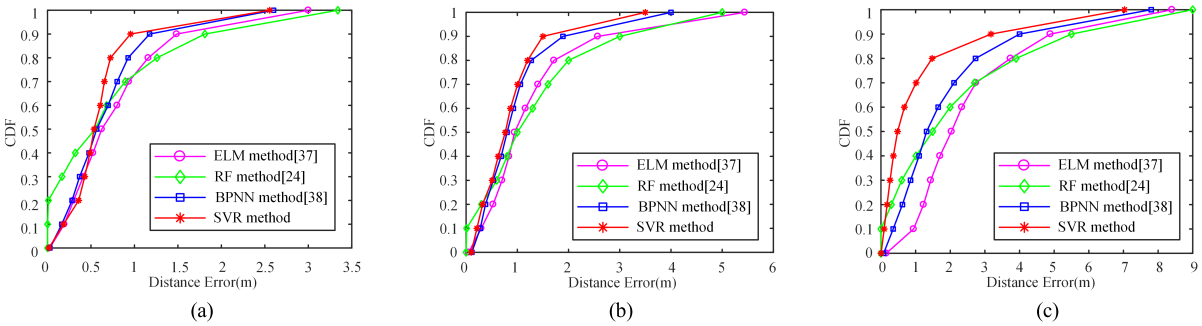

FIGURE 10. CDF of different algorithms in three environments. (a) Empty room. (b) Conference room. (c) Corridor.

subcarriers. The combination of statistical and network features can more comprehensively characterize the mapping relationship between fingerprint information and location, which also verifies the content of V-B-1). In addition, the proposed method in this paper outperforms the [30], which demonstrates that LPHVG outperforms VG in characterizing the correlation between subcarriers.

3) COMPARISON OF DIFFERENT MACHINE LEARNING ALGORITHMS

Different machine learning algorithms lead to various localization performances. We analyze the localization performance of four algorithms, RF [24], extreme learning machine (ELM) [37], back propagation neural network (BPNN) [38], and SVR. Fig. 10(a)-(c) shows the CDF of different algorithms in three environments. From the figure, it can be seen that the error of 80% of the test data of the SVR method used in this paper can be controlled within 0.7m in the empty room, while the positioning accuracy of ELM method, RF method, and BPNN method are 1.2m, 1.3m and 0.8m respectively under this percentage; 80% of the SVR method used in this paper can be controlled within 0.7m in the conference room. The error of the test data can be controlled within 1m, while the positioning accuracy of ELM, RF, and BPNN methods are 1.8m, 2 m, and 1.1m respectively under this percentage; in the corridor, the error of 80% of the test data can be controlled within 1.5m with SVR method, while the positioning accuracy of ELM, RF and BPNN methods is 3.5m, 3.5m and 3.1m respectively under this percentage. The statistics of the localization errors of different machine learning algorithms in the three environments are shown in Table 3. The results show that the average and median errors of the SVR method are lower than those of the other methods under different experimental environments. It can be seen that the SVR localization method based on the combination of LPHVG and Statistics proposed in this paper has the

TABLE 3. Localization errors of different algorithms (meters).

	Empty Room		Conference Room		Corridor	
	Mean	Median	Mean	Median	Mean	Median
ELM [37]	0.805	0.623	1.035	1.010	2.214	2.036
RF [24]	0.711	0.548	0.916	0.892	1.869	1.495
BPNN [38]	0.646	0.566	0.895	0.787	1.804	1.317
SVR	**0.596**	**0.535**	**0.837**	**0.755**	**1.270**	**0.579**

best localization performance. BPNN utilizes the gradient search technique to continuously correct the obtained results, which has a strong nonlinear mapping capability. Still, the convergence speed is slow and brings high running time to the system. ELM obtained the weights between the input and hidden layers and the thresholds of the nodes in the hidden layer by random initialization based on the traditional feedforward neural network, which significantly improved the learning rate. Still, the performance varied significantly due to the random generation of the weight parameters and the poor localization. RF has high classification accuracy in current machine learning algorithms but can overfit regression problems for specific data sets. SVR minimizes the empirical risk and confidence range by seeking structured risk minimization, has good generalization and fitting ability, and has better performance for high-dimensional data. It can be concluded that the method proposed in this paper has good localization performance in different environments and has some anti-interference ability for complex environments.

4) PERFORMANCE ANALYSIS IN MULTIPLE SCENARIOS

As can be seen from the above, the average error and median error of the method proposed in this paper are 0.596m and 0.535m in the empty room, 0.837m and 0.755m in the conference room, and 1.270m and 0.579m in corridor. In the empty room, the noise and interference are less, and the environment is more ideal, so the higher positioning accuracy is achieved. The environment of the conference room is complex, with various tables, chairs and other sundry objects placed indoors, which has rich multipath effect, which will have a great impact on the positioning accuracy. Therefore, the positioning accuracy under the conference room is lower than that of the empty room. In the corridor, the experimental environment is narrow and slender, which greatly interferes with signal transmission. At the same time, to make the experimental environment more similar to the actual application scene, we arrange for a volunteer to pass through the corridor every minute. Therefore, the positioning error of the corridor is large in the three environments.

5) PERFORMANCE ANALYSIS OF DIFFERENT LITERATURE

To verify the effectiveness of the algorithm, we compared the algorithm proposed in this paper with LCAF [39] and reference [40] under the same experimental conditions. As shown in Fig. 11, the proposed algorithm can control the error

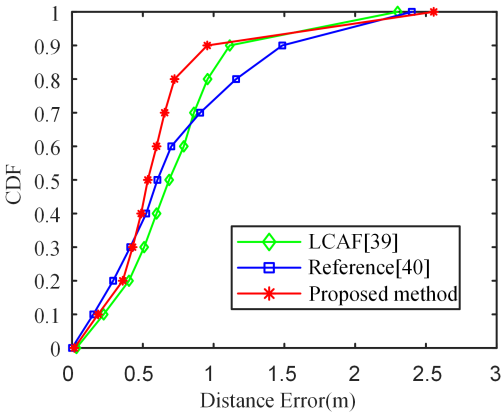

FIGURE 11. CDF of different literature.

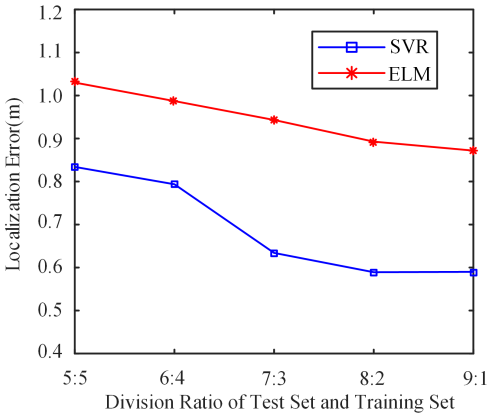

FIGURE 12. The effect of division ratio on localization performance.

of 80% of the test data within 0.7m, while the positioning accuracy of LCAF and literature 40 within 80% error is 0.9m and 1.2m, respectively. LCAF first eliminates the noise interference by pre-processing method, then generates more stable fingerprints by linear discriminant analysis (LDA), and finally determines the estimated target localization by using the plain Bayesian-based algorithm. Reference [40] uses split-averaging and principal component analysis (PCA) methods to reduce the dimensionality of the data, and weighted k-nearest neighbors (WKNN) for location estimation. These two methods enhance the fingerprint from different perspectives, but both ignore the location information contained between subcarriers. In this paper, we fully exploit the relationship between subcarriers and construct

TABLE 4. Localization errors of amplitude, phase, and both (meters).

	Empty Room		Conference Room		Corridor	
	Mean	Median	Mean	Median	Mean	Median
Amplitude	0.823	0.715	1.110	1.017	1.440	1.276
Phase	0.792	0.655	1.121	1.026	1.509	1.310
Both	**0.596**	**0.535**	**0.837**	**0.755**	**1.270**	**0.579**

fingerprints using network features and statistical features. The results show that the proposed algorithm in this paper exhibits optimal performance.

C. EFFECT OF PARAMETERS ON LOCALIZATION

This subsection discusses the selection of amplitude and phase, the ratio of training set and test set division, and the selection of grid resolution, respectively.

1) EFFECT OF AMPLITUDE AND PHASE

Table 4 shows the average localization errors using amplitude, phase, and both in the three environments. We can see that using both can effectively improve the localization accuracy. Because amplitude and phase represent CSI in different ways, utilizing both can increase the available localization information and thus improve the localization performance of the algorithm.

2) EFFECT OF TRAINING SET AND TEST SET DIVISION RATIO

To verify the effect of the training set and test set size on the performance of the algorithms, simulation validation is made under different ratios of division. This paper gives the simulation results of the average error under the ratios of 5:5, 6:4, 7:3, 8:2, and 9:1 based on SVR and ELM, respectively. As shown in Fig. 12, the performance of the two algorithms improves as the percentage of the training set increases, reaching the best at 8:2 and 9:1. However, when the entire sample set is not large enough, the number of samples in the test set is too small. For example, when the total number of samples is 100, only 10 test samples are obtained at a ratio of 9:1, and such a small sample of data makes the results not generalizable. And the prediction results are not generalized, which may lead to overfitting the algorithm and reduce the system performance. Therefore, this paper finally chooses to divide the training set and test set in the ratio of 8:2.

3) EFFECT OF GRID RESOLUTION

To evaluate the effect of different resolution grids on the localization results, comparative analyses are performed in the empty room for grids of 0.6m $\times$ 0.6m, 0.8m $\times$ 0.8m, 1.5m $\times$ 1.5m, and 2m $\times$ 2m sizes, respectively. Fig. 13 shows the CDF of four different resolution grid cases. We can see that the lower the grid resolution is, the larger the positioning error is, and increasing the grid resolution can help improve the positioning accuracy. However, when the resolution reaches a certain accuracy, it has almost no effect on the positioning performance. For example, 0.6m $\times$ 0.6m and 0.8m $\times$ 0.8m grids get almost the same positioning accuracy. At the same time, too high a resolution leads to an increase in deployment cost and algorithm complexity. We want to find a compromise between localization accuracy and deployment cost. Therefore, considering the relationship between localization cost and localization accuracy, the 0.8m $\times$ 0.8m size is used as the grid resolution in this paper.

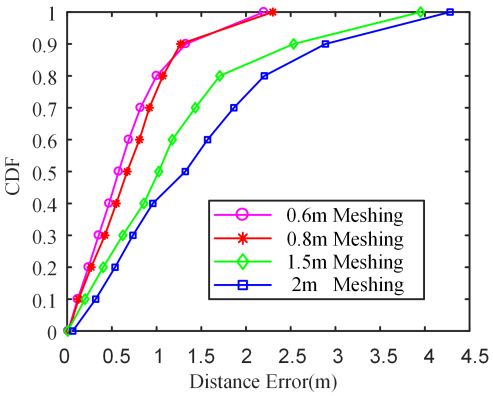

FIGURE 13. CDF of different grid resolution.

VI. CONCLUSION

In this paper, we proposed a device-free indoor localization method based on LPHVG and CSI. The method achieves high localization performance by mining the location information between subcarriers and utilizing the statistical features within subcarriers and network features between subcarriers under the premise that a single AP and the tested object do not need to carry equipment. The central idea is to utilize the LPHVG algorithm to convert the amplitude and phase information of CSI into a complex network and extract network features, and then combine the network features with the traditional statistical features to determine the specific location based on SVR. We performed analysis and validation in different environments and compare with different methods. The results show that the method outperforms existing localization methods and has an excellent performance in different environments.

REFERENCES

[1] P. Enge and P. Misra, "Special issue on global positioning system," *Proc. IEEE*, vol. 87, no. 1, pp. 3–15, Jan. 1999.
[2] S. Dhar and U. Varshney, "Challenges and business models for mobile location-based services and advertising," *Commun. ACM*, vol. 54, no. 5, pp. 121–128, May 2011.

[3] W. Liu, H. Chen, Z. Deng, X. Zheng, X. Fu, and Q. Cheng, "LC-DNN: Local connection based deep neural network for indoor localization with CSI," *IEEE Access*, vol. 8, pp. 108720–108730, 2020.
[4] A. Bochem and H. Zhang, "Robustness enhanced sensor assisted Monte Carlo localization for wireless sensor networks and the Internet of Things," *IEEE Access*, vol. 10, pp. 33408–33420, 2022.
[5] Y. Zhang, W. Wang, C. Xu, J. Qin, S. Yu, and Y. Zhang, "SICD: Novel single-access-point indoor localization based on CSI-MIMO with dimensionality reduction," *Sensors*, vol. 21, no. 4, p. 1325, Feb. 2021.
[6] K. Wu, J. Xiao, Y. Yi, D. Chen, X. Luo, and L. M. Ni, "CSI-based indoor localization," *IEEE Trans. Parallel Distrib. Syst.*, vol. 24, no. 7, pp. 1300–1309, Jul. 2013.
[7] P. Malekzadeh, A. Mohammadi, M. Barbulescu, and K. N. Plataniotis, "STUPEFY: Set-valued box particle filtering for Bluetooth low energy-based indoor localization," *IEEE Signal Process. Lett.*, vol. 26, no. 12, pp. 1773–1777, Dec. 2019.
[8] E. DiGiampaolo and F. Martinelli, "Multiple baseline synthetic array for UHF RFID localization," in *Proc. IEEE Int. Conf. RFID Technol. Appl. (RFID-TA)*, Sep. 2019, pp. 348–352.
[9] P. K. Yoon, S. Zihajehzadeh, B.-S. Kang, and E. J. Park, "Robust biomechanical model-based 3-D indoor localization and tracking method using UWB and IMU," *IEEE Sensors J.*, vol. 17, no. 4, pp. 1084–1096, Feb. 2017.
[10] Y. Shu, C. Bo, G. Shen, C. Zhao, L. Li, and F. Zhao, "Magicol: Indoor localization using pervasive magnetic field and opportunistic WiFi sensing," *IEEE J. Sel. Areas Commun.*, vol. 33, no. 7, pp. 1443–1457, May 2015.
[11] K. Yang, Z. Liang, R. Liu, and W. Li, "RSS-based indoor localization using min-max algorithm with area partition strategy," *IEEE Access*, vol. 9, pp. 125561–125568, 2021.
[12] Y. Sun, S. Yang, G. Wang, and H. Chen, "Robust RSS-based source localization with unknown model parameters in mixed LOS/NLOS environments," *IEEE Trans. Veh. Technol.*, vol. 70, no. 4, pp. 3926–3931, Apr. 2021.
[13] P. Bahl and V. N. Padmanabhan, "RADAR: An in-building RF-based user location and tracking system," in *Proc. 19th Annu. Joint Conf. IEEE Comput. Commun. Societies*, Mar. 2000, pp. 775–784.
[14] M. Youssef and A. Agrawala, "The Horus WLAN location determination system," in *Proc. 3rd Int. Conf. Mobile Syst., Appl., Services (MobiSys)*, Jun. 2005, pp. 205–218.
[15] D. Halperin, W. Hu, A. Sheth, and D. Wetherall, "Predictable 802.11 packet delivery from wireless channel measurements," *ACM SIGCOMM Comput. Commun. Rev.*, vol. 40, no. 4, pp. 159–170, 2010.
[16] Y. Lv, N. Wie, and K. Li, "Construction of multiplex muscle network for precision pinch force control," in *Proc. 42nd Annu. Int. Conf. IEEE Eng. Med. Biol. Soc. (EMBC)*, Jul. 2020, pp. 3269–3272.
[17] J. Xiao, K. Wu, Y. Yi, and L. M. Ni, "FIFS: Fine-grained indoor fingerprinting system," in *Proc. 21st Int. Conf. Comput. Commun. Netw. (ICCCN)*, Jul. 2012, pp. 1–7.
[18] X. Wang, L. Gao, S. Mao, and S. Pandey, "DeepFi: Deep learning for indoor fingerprinting using channel state information," in *Proc. IEEE Wireless Commun. Netw. Conf. (WCNC)*, Mar. 2015, pp. 1666–1671.
[19] X. Dang, X. Si, Z. Hao, and Y. Huang, "A novel passive indoor localization method by fusion CSI amplitude and phase information," *Sensors*, vol. 19, no. 4, p. 875, Feb. 2019.
[20] X. Wang, L. Gao, and S. Mao, "BiLoc: Bi-modal deep learning for indoor localization with commodity 5 GHz WiFi," *IEEE Access*, vol. 5, pp. 4209–4220, 2017.
[21] D. Man, L. Bing, and J. Lv, "Indoor localization algorithm based on attribute-independent weighted naive Bayesian," in *Proc. Int. Conf. Cyberspace Innov. Adv. Technol.*, Dec. 2020, pp. 202–207.
[22] Y. Wang, C. Xiu, X. Zhang, and D. Yang, "WiFi indoor localization with CSI fingerprinting-based random forest," *Sensors*, vol. 18, no. 9, p. 2869, Aug. 2018.
[23] Z. Wu, Q. Xu, J. Li, C. Fu, Q. Xuan, and Y. Xiang, "Passive indoor localization based on CSI and naive Bayes classification," *IEEE Trans. Syst., Man, Cybern., Syst.*, vol. 48, no. 9, pp. 1566–1577, Sep. 2018.
[24] Z. H. Wu, Y. Han, Y. Chen, and K. J. R. Liu, "A time-reversal paradigm for indoor positioning system," *IEEE Trans. Veh. Technol.*, vol. 64, no. 4, pp. 1331–1339, Apr. 2015.
[25] C. Chen, Y. Chen, Y. Han, H.-Q. Lai, F. Zhang, and K. J. R. Liu, "Achieving centimeter-accuracy indoor localization on WiFi platforms: A multi-antenna approach," *IEEE Internet Things J.*, vol. 4, no. 1, pp. 122–134, Feb. 2017.
[26] H. Zhu, F. Xiao, L. Sun, R. Wang, and P. Yang, "R-TTWD: Robust device-free through-the-wall detection of moving human with WiFi," *IEEE J. Sel. Areas Commun.*, vol. 35, no. 5, pp. 1090–1103, May 2017.
[27] L. Lacasa, B. Luque, F. Ballesteros, J. Luque, and J. C. Nuño, "From time series to complex networks: The visibility graph," *Proc. Nat. Acad. Sci. USA*, vol. 105, no. 13, pp. 4972–4975, Apr. 2008.
[28] J. Iacovacci and L. Lacasa, "Visibility graphs for image processing," *IEEE Trans. Pattern Anal. Mach. Intell.*, vol. 42, no. 4, pp. 974–987, Apr. 2020.
[29] Z. Wu, X. Pan, K. Fan, K. Liu, and Y. Xiang, "Device-free orientation detection based on CSI and visibility graph," *IEEE Trans. Syst., Man, Cybern., Syst.*, vol. 51, no. 7, pp. 4433–4442, Jul. 2021.
[30] Z. Wu, L. Jiang, Z. Jiang, B. Chen, K. Liu, Q. Xuan, and Y. Xiang, "Accurate indoor localization based on CSI and visibility graph," *Sensors*, vol. 18, no. 8, p. 2549, Aug. 2018.
[31] B. Luque, L. Lacasa, F. Ballesteros, and J. Luque, "Horizontal visibility graphs: Exact results for random time series," *Phys. Rev. E, Stat. Phys. Plasmas Fluids Relat. Interdiscip. Top.*, vol. 80, no. 4, Oct. 2009, Art. no. 046103.
[32] S. S. Roy and S. Chatterjee, "Partial discharge detection framework employing spectral analysis of horizontal visibility graph," *IEEE Sensors J.*, vol. 21, no. 4, pp. 4819–4826, Feb. 2021.
[33] Y. B. Luo, B. F. Zhang, B. S. Wang, X. M. Chen, and Y. P. Sun, "FL-LPVG: An approach for anomaly detection based on flow-level limited penetrable visibility graph," in *Proc. Int. Conf. Inf. Netw. Secur. (ICINS)*, 2013, pp. 1–7.
[34] M. Kotaru, K. Joshi, D. Bharadia, and S. Katti, "SpotFi: Decimeter level localization using WiFi," in *Proc. ACM Conf. Special Interest Group Data Commun.*, 2015, vol. 45, no. 4, pp. 269–282.
[35] M. E. J. Newman, "Mixing patterns in networks," *Phys. Rev. E, Stat. Phys. Plasmas Fluids Relat. Interdiscip. Top.*, vol. 67, no. 2, Feb. 2003, Art. no. 026126.
[36] R. Zhou, J. Chen, X. Lu, and J. Wu, "CSI fingerprinting with SVM regression to achieve device-free passive localization," in *Proc. IEEE 18th Int. Symp. World Wireless, Mobile Multimedia Netw. (WoWMoM)*, Jun. 2017, pp. 1–9.
[37] J. Xue, Z. Gao, J. Zhang, and W. Xiao, "Device-free localization using extreme learning machine with DTW based feature extraction," in *Proc. Int. Conf. Commun., Inf. Syst. Comput. Eng. (CISCE)*, May 2021, pp. 239–242.
[38] M. Zhou, Y. Long, W. Zhang, Q. Pu, Y. Wang, W. Nie, and W. He, "Adaptive genetic algorithm-aided neural network with channel state information tensor decomposition for indoor localization," *IEEE Trans. Evol. Comput.*, vol. 25, no. 5, pp. 913–927, Oct. 2021.
[39] D. Liu, Z. Liu, and Z. Song, "LDA-based CSI amplitude fingerprinting for device-free localization," in *Proc. Chin. Control Decis. Conf. (CCDC)*, Aug. 2020, pp. 2020–2023.
[40] J. Fan, J. Zhang, and X. Dou, "Single-site indoor fingerprint localization based on MIMO-CSI," *China Commun.*, vol. 18, no. 8, pp. 199–208, Aug. 2021.

YING LIU was born in 1983. She received the Ph.D. degree in communication and information system from Jilin University, in 2011. She is currently an Associate Professor with Liaoning Technical University. Her research interests include wireless positioning and intelligent wireless sensing.

GUOQING LI received the B.S. degree in communication engineering from Liaoning Technical University, Huludao, China, in 2020, where he is currently pursuing the M.S. degree. His main research interest includes fingerprint positioning.